RSC Advances

PAPER

View Article Online
View Journal | View Issue



Cite this: *RSC Adv.*, 2025, **15**, 5720

# Alkali metal lithium doping promotes the high stability and ionic kinetics of cathode materials for sodium-ion batteries†

Weiping Shu,[a] Lili Wang,[a]* Siqiang Zhang,[a] Ye Liu[a] and Qiang Han[b]

Layered transition metal oxides for sodium-ion batteries are regarded as the most promising cathode materials for commercialization owing to their high theoretical specific capacity, high rate performance, and low cost. However, their drawbacks, such as unfavorable phase transitions, $Na^+$/vacancy disorder, and slow dynamics, seriously hinder their further practical applications. In this work, we prepared a P2-$Na_{0.67}Ni_{0.1}Co_{0.1}Mn_{0.8}O_2$ cathode with a heteroatom-substitution doped at the alkali metal position. The unfavorable phase transition was suppressed to a certain extent, and the order of $Na^+$/vacancy was optimized. The initial discharge-specific capacity of the prepared $[Na_{0.57}Li_{0.1}]Ni_{0.1}Co_{0.1}Mn_{0.8}O_2$ at 0.1C (1C = 150 mA h $g^{-1}$) was 151.3 mA h $g^{-1}$. Doping with the alkali metal Li enhanced the stability of the layered structure, resulting in an improvement in cycling performance, and the capacity retention rate reached 87.9% after 100 cycles. In addition, the material had a stable structure and excellent $Na^+$ diffusion coefficient at a high current density of 10C. It also exhibited an excellent rate capacity of 88.2 mA h $g^{-1}$ in an Na half-cell system. Kinetic analysis showed that the increase in $Na^+$ diffusion rate was due to the increase in the $Na^+$/vacancy disorder and the rise in Na interlayer spacing.

Received 4th November 2024
Accepted 26th December 2024

DOI: 10.1039/d4ra07855a

rsc.li/rsc-advances



## Introduction

Lithium-ion batteries have been widely used in portable power products and electric vehicle markets owing to their advantages of high voltage, long cycle life, and environmental friendliness.[1,2] However, high costs and fossil energy consumption issues limit the further development of lithium-ion batteries.[3] In recent years, sodium-ion batteries (SIBs) have been the best choice to ensure ideal charge–discharge capacity and cycling performance at low cost.[4–6] In addition to safety, cost, and electrochemical performance, capacity retention is an important factor for their wide practical applications in the commercial market.[7]

Generally, the irreversible phase transition during the charging and discharging of a battery, Jahn–Teller lattice distortion of $Mn^{3+}$, and $Na^+$/vacancy ordering are the main reasons for the degradation of SIB's electrochemical performance.[8,9] Methods including elemental doping and encapsulation have been extensively studied to mitigate the structural changes during cycling. Single-atom cation doping[10] using ions, such as $Mg^{2+}$, $Co^{2+}$, $Ni^{2+}$, and $Ti^{4+}$, has been proven to be an effective method to improve the performance of the cathode materials.[11–14] During the charge and discharge process of the battery, sodium ions continue to migrate between the electrolyte and the electrode material. The specific capacities can severely deteriorate when the rate reaches 2C or higher.[15–17] The high rate limit can be attributed to the burst of concentrated sodium ions to the negative electrode surface in a short period, forming concentration polarization with the low sodium ion concentration in the electrolyte, and the side effects of this ohmic polarization will be amplified under high current conditions, causing the battery voltage to drop instantaneously, and at the same time, the diffusion rate of sodium ions is limited.[18] Electrodes with stable three-dimensional skeleton structures, such as polyanionic battery materials, $Na_3Ti_{0.5}V_{0.5}(PO_3)_3N$,[19] $Na_3V_{1.5}Cr_{0.5}(PO_4)_3$ (ref. 20) and $Na_3MnTi(PO_4)_3$,[21] are the first choice for high-rate applications. However, polyanionic materials have defects such as low conductivity and large volume changes during cycling, and the lack of suitable experimental protocols for modifications hinders their commercial application. Hence, there is an urgent need to develop electrode materials that can achieve optimal battery performance at high speeds. Researchers have widely considered layered oxides owing to their high energy density, good cycling stability, high operating voltage, diverse structures, and mature synthesis methods. Consequently, it has become the best choice for sodium ion cathode material.

We studied P2-$Na_{0.67}MnO_2$ co-doped with Li (alkali metal site), Ni, and Co, revealing the optimization effect of Li doping

[a]*School of Mathematics, Physics and Statistics, Shanghai University of Engineering Science, Shanghai, 201620, China. E-mail: swpingyes@gmail.com; llwang@sues.edu.cn*

[b]*Office of Science and Development, Shanghai Donghai Vocational and Technical College, Shanghai, 200241, China*

† Electronic supplementary information (ESI) available. See DOI: https://doi.org/10.1039/d4ra07855a

at the alkali metal site and the synergistic effect between Li and diatoms. In this work, we chose the manganese-rich system of the P2 phase to demonstrate the structural changes under Li doping. In $Na_{0.67}Ni_{0.1}Co_{0.1}Mn_{0.8}O_2$ (NNCM), the alkali metal site is doped with $Li^+$ with a smaller radius, which helps to suppress the $Na^+$/vacancy ordering of the system.[22–26] Li will preferentially occupy the Na site of the alkali metal layer, while a small portion of Li will enter the transition metal layer to replace the Mn site. Synergistically with the two doped transition metal elements, it can suppress the Jahn–Teller distortion caused by $Mn^{3+}$ and improve the structural stability.[27] At the same time, the distance between the $TMO_2$ layers is increased,[28,29] providing a better channel for the rapid migration of $Na^+$. The prepared $[Na_{0.57}Li_{0.1}]Ni_{0.1}Co_{0.1}Mn_{0.8}O_2$ ([NL]NCM) sample has an initial discharge specific capacity of 151.3 mA h $g^{-1}$ at 0.1C, and the capacity retention rate after 100 cycles is as high as 87.9%. It has excellent rate performance of 88.2 mA h $g^{-1}$ at 10C.

## Materials and methods

### Preparation of the substrate

The P2 type [NL]NCM cathode material was prepared using a typical sol–gel method. 17 mmol of citric acid was dissolved in 50 mL water, and sodium acetate trihydrate, manganese acetate tetrahydrate, nickel acetate tetrahydrate, cobalt acetate tetrahydrate, and lithium acetate dihydrate were added to the acid solution according to the stoichiometric ratio according to the proportions of different substances. The total amount was 17 mmol. The solution was heated to 80 °C with continuous stirring for 30 minutes to evaporate the water from the solution. Subsequently, the precursor was placed in an electric constant-temperature blast drying oven and dried at 70 °C for 24 hours. The pink [NL]NCM sample was taken out and ground into a powder with fine and uniform particles using a mortar rod. For [NL]NCM, it was kept in an air environment at 500 °C for 12 hours and then calcined at 900 °C for 10 hours. Finally, the [NL]NCM sample was obtained by naturally cooling to room temperature. The synthesis procedure is shown in Fig. 1.

### Characterization

The crystalline phases of compounds were investigated through powder X-ray diffraction (XRD) on a D8 X-ray diffractometer using Cu Kα radiation. The morphology and microstructure of the as-prepared materials were analyzed through field-emission scanning electron microscopy (SEM, ZEISS Gemini SEM 300, 15 kV) and transmission electron microscopy (TEM, FEI Tecnai G2 F20, 200 kV). Surface chemistry states were determined using X-ray photoelectron spectroscopy (XPS, Thermo Scientific K-Alpha XPS).

### Electrochemical characterization

Cathodes were fabricated by blending active materials (80 wt%), super P carbon black (10 wt%), and polyvinylidene fluoride (10 wt%). Then, the resulting slurry was coated on aluminum

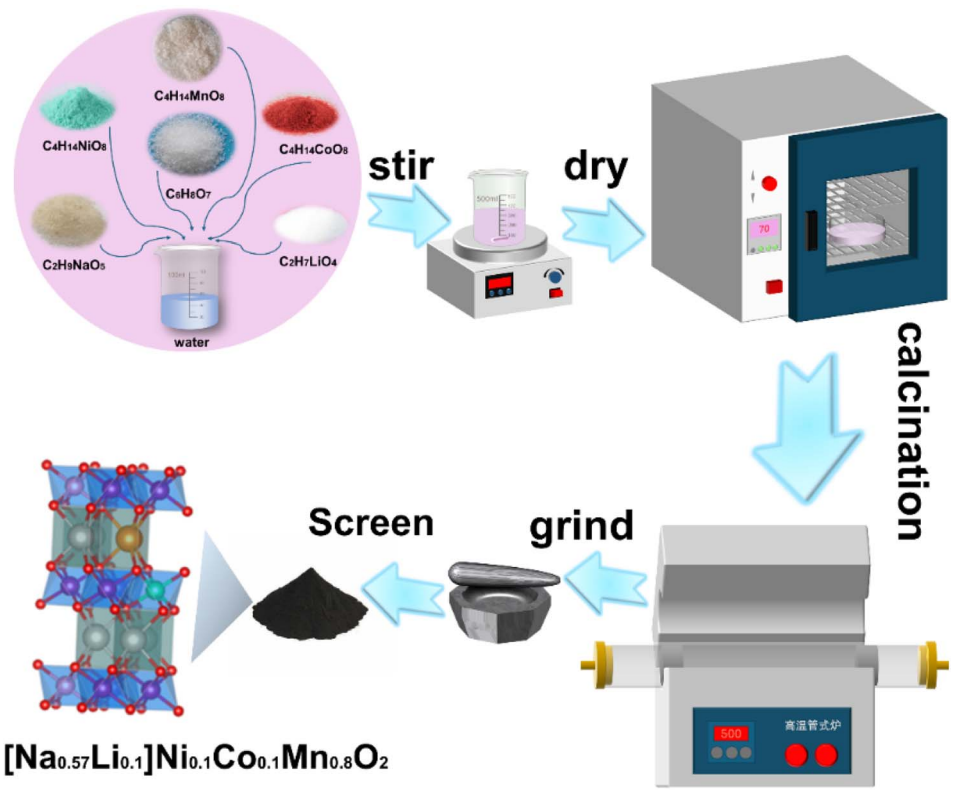


Fig. 1 Synthesis process of the $[Na_{0.57}Li_{0.1}]Ni_{0.1}Co_{0.1}Mn_{0.8}O_2$ cathode material.

foil and dried in a vacuum drying oven at 80 °C for over 12 hours. The mass loading of the active substance was 1–1.3 mg $cm^{-2}$. Half cells were assembled with 2032 type-coin cells in an Ar-containing dry box. The Na metal was the anode and the electrolyte was composed of 1 mol per L $NaPF_6$ in a solution of ethylene carbonate and propylene carbonate (volume ratio of 1 : 1) with 5% fluoroethylene carbonate. Electrochemical tests, including charge/discharge performance analyses, were conducted using the NEWARE battery test system (CT-3008) at room temperature. All batteries were set aside for about 10 hours before testing to equalize. Cyclic voltammetry (CV) and impedance measurements were measured on the electrochemical station (NEWARE) by applying a 0.2 mV harmonic perturbation signal. Electrochemical impedance spectroscopy (EIS) spectra were acquired at the frequency of 0.01 Hz to 10 kHz.

## Results and discussion

To reveal the synergistic effect of alkali metal site doping and transition metal site heteroatom doping, P2-[NL]NCM was synthesized by doping alkali metal site Li. Fig. 2a and b reveal the powder X-ray diffraction (XRD) peaks of [NL]NCM. The diffraction peaks of the XRD pattern belong to the typical hexagonal structure (space group: $P6_3/mmc$). After doping Li at the alkali metal site, a cubic spinel phase appeared with the space group $Fd\bar{3}m$. It can be seen from the changes in the lattice parameters that the alkali metal Li doping affects the layered structure of P2. The (002) peak of [NL]NCM shifts to a large angle relative to NNCM (Fig. 2c). As seen in Fig. 2d and Table S1,† the lattice parameter $c$ of the interlayer spacing decreases from 11.267 to 11.200, at the same time, both $a$ and $b$ decreased from 2.88 to 2.85, which is because the sodium at the alkali metal site is replaced by lithium; results show that the Na atoms in the lattice have a larger radius ($\approx$1.02 Å) and are partially replaced by Li atoms ($\approx$0.76 Å), successfully, with a smaller radius, resulting in unit cell shrinkage, so lithium doping at the alkali metal site can expand the spacing between the sodium layers.[30]

To further study the surface composition of modified NNCM, X-ray photoelectron spectroscopy (XPS) analysis was performed on NNCM and [NL]NCM materials. Fig. 2e shows the XPS full spectrum of the [NL]NCM cathode material, and Fig. 2d and S1† confirm the oxidation state of Mn. The Mn 2p spectra of the two materials are similar, and the binding energy of Mn is between that of the trivalent (Mn $2p_{3/2}$, 641.2 eV) and tetravalent (Mn $2p_{3/2}$, 642.5 eV) manganese states.[31,32] The concentration of $Mn^{3+}$ in [NL]NCM (48%) is lower than that in NNCM (62%); due to the

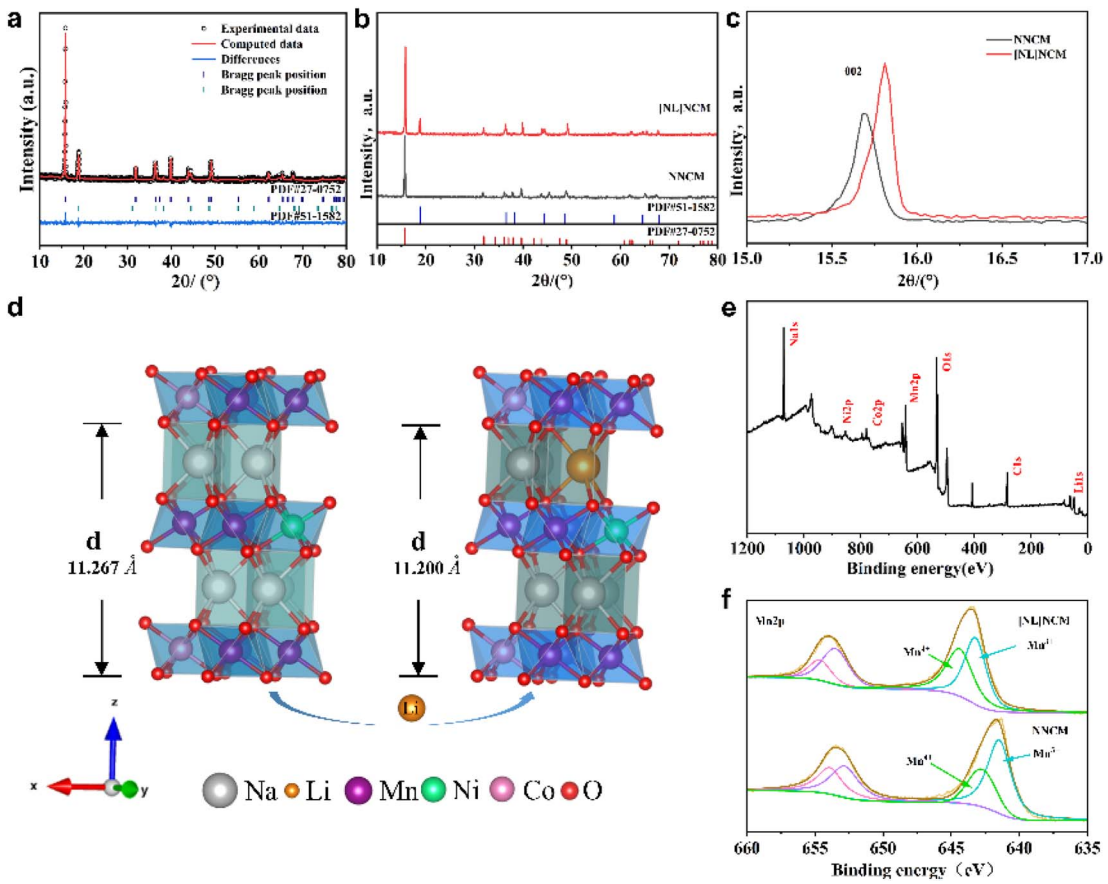


Fig. 2 Material characterization of NNCM and [NL]NCM: (a) Rietveld refinement results of the [NL]NCM powder (b) XRD patterns of the pristine NNCM and [NL]NCM (c) magnified patterns of the two samples between 15° and 17°. (d) Schematic of the effect of Li doping on the electrode structure (e) XPS full spectrum of [NL] NCM and (f) Mn 2p XPS fitted spectra of NNCM and [NL]NCM powders.

charge compensation mechanism, a small amount of Li enters the transition metal layer to replace the manganese site, causing high-spin $Mn^{3+}$ to be oxidized to $Mn^{4+}$. The bond energy of the Li–O bond (−561.2 kJ $mol^{-1}$) is higher than the bond energy of the Mn–O bond in [NL]NCM (−465.2 kJ $mol^{-1}$), indicating that Li doping can improve the stability of the structure.

To analyze the visualized microstructure of NNCM and [NL]NCM powders, The morphology and crystal structure information were acquired through SEM and TEM, as shown in Fig. 3a and S2.† The [NL]NCM particles exhibited a micro flake structure with a thickness of about 2 μm, which has a similar morphology to NNCM, which indicates that the addition of alkali metal Li, has little effect on the shape of the composite. The widths between the measured adjacent lattice fringes are approximately 4.75 and 4.1 Å, respectively, for the (111) and (200) planes of the granular layered hexagonal structure (Fig. 3b–d). Selective region electron diffraction (SAED) further confirmed that the TM atoms were arranged in a typical hexagonal symmetry phase. In addition, the energy spectrum (EDS) showed that the Ni, Co, Mn, and O elements in the [NL]NCM cathode material were uniformly distributed, and the uneven Na arrangement may be due to the alkali doping of Li, which improves the disorder of $Na^+$/vacancy.[24] (Fig. 3e–i)

The electrochemical performance of Na-ion half cells using NNCM, and [NL]NCM compounds as positive electrodes was systematically tested under normal temperature conditions. Fig. 4a and S3a† show the CV curves of [NL]NCM and NNCM for the first 3 cycles in a Na-ion half-cell, scanning between 1.5–4.2 V at a rate of 0.2 mV $s^{-1}$, and each cycle of [NL]NCM showed good stability and reversibility. In the low-voltage region around 2.0 V, the redox peak is the redox process of $Mn^{3+}/Mn^{4+}$, and the redox peak in the high-voltage region may be related to the reversible redox reaction of cobalt.

With the addition of Li at the alkali metal site, the redox peak intensity of the material in the high-pressure region is significantly reduced, the two voltage platforms completely disappear, the capacity is not reduced, and only one broad redox peak is observed in the CV test of [NL]NCM. It shows that when Li is added to the alkali metal layer, the ordering of $Na^+$/vacancies is effectively suppressed during the charge and discharge process. The initial three charge–discharge curves of the [NL]NCM positive electrode are shown in Fig. 4b, which was tested under the conditions of 1.5–4.2 V and 0.2C. During the initial charging process, a slope of 2.9–4.2 V and a voltage plateau of around 4.2 V were shown, which is consistent with the CV results. Compared with the initial three charge–discharge curves of NNCM (Fig. S3b†), sample [NL]NCM exhibits smaller polarization and better reversibility, which may be due to the effect of Li doping.

The initial discharge-specific capacity of the [NL]NCM sample in the first discharge cycle is 146 mA h $g^{-1}$, and the

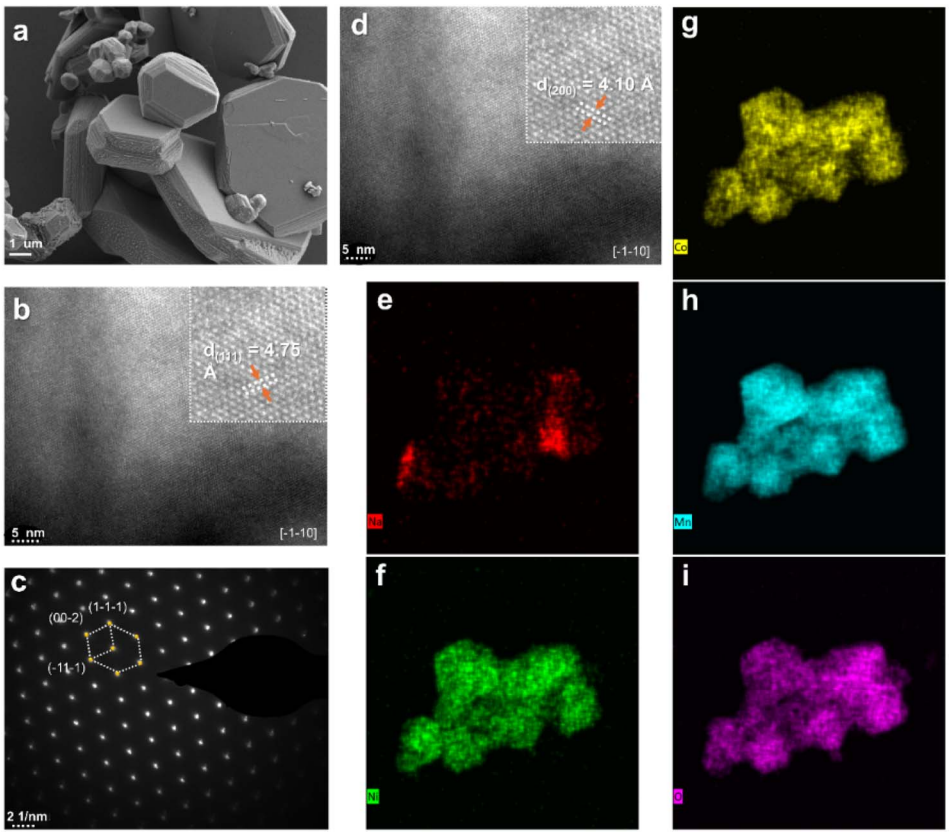


Fig. 3 Structural characterization of [NL]NCM material: (a) SEM (b–d) HRTEM image at the [−1−10] zone axis and the corresponding SAED image (e–i) TEM (HAADF Na, Ni, Co, Mn, and O) elemental mapping images of the [NL]NCM powder.

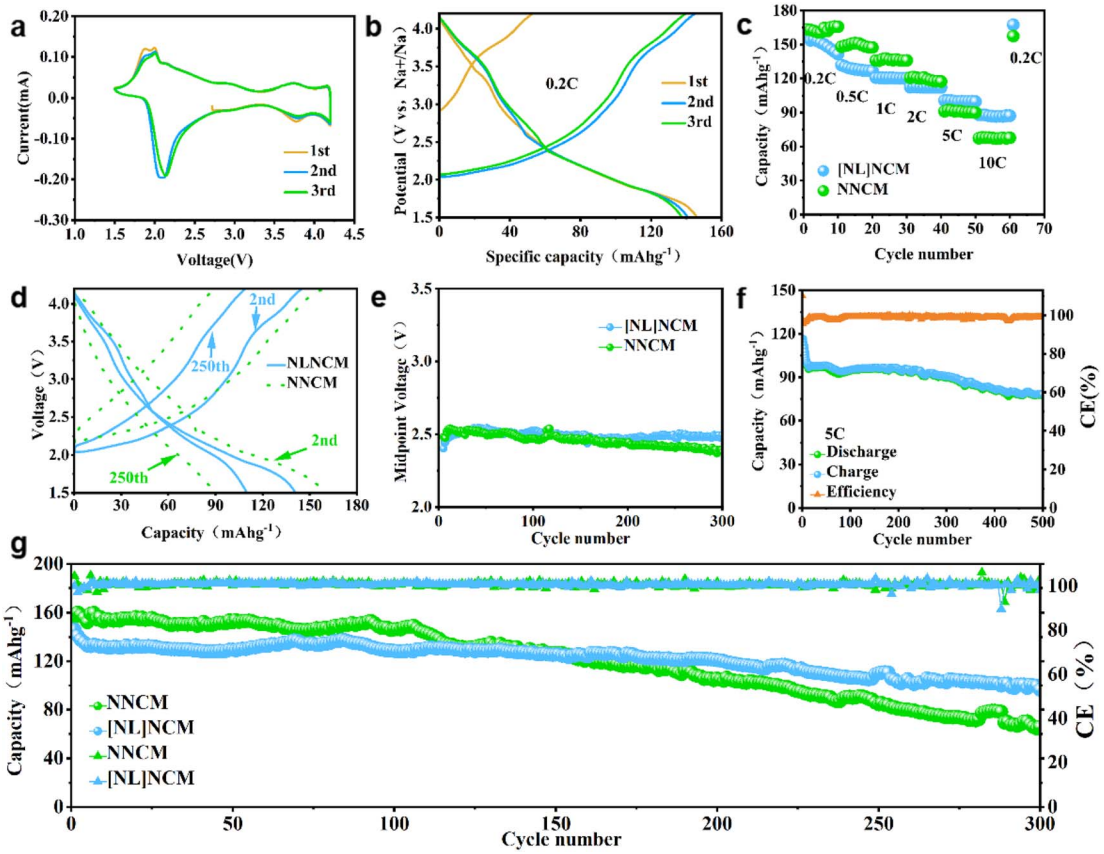


Fig. 4 Electrochemical properties: (a) CV curves of [NL]NCM. (b) Initial three charges/discharges. (c) Rate capabilities at different rates. (d) Second to 250th voltage profiles at 0.2C. (e) Midpoint voltage of discharge at 0.2C. (f) Long cycling performance of [NL]NCM at 5C, and (g) cycling performance of NNCM and [NL]NCM at 0.2C.

discharge slopes are 4.2–1.75 and 1.75–1.5 V, respectively. The initial discharge-specific capacity of the NNCM sample is 156 mA h $g^{-1}$. As shown in Fig. 4c, when the electrode was cycled at different current densities from 0.2C to 10C, the reversible capacities of [NL]NCM were approximately 158.7, 131.8, 120.6, 112.5, 100.7 and 88.2 mA h $g^{-1}$, while for the original material at 0.2C, 0.5C, 1C, 2C, 5C and 10C, the discharge capacities were 163.4, 148.0, 135.9, 120.5, 91.2 and 67.4 mA h $g^{-1}$, respectively. When returning to the initial low current density, the P2-type [NL]NCM cathode could still provide a high capacity of 167.4 mA h $g^{-1}$, indicating good reversibility over a wide current density range. Fig. 4d compares the cycling performance of the two samples. After 250 cycles, the discharge-specific capacities of the cathode materials are 101.2 mA h $g^{-1}$ and 84.6 mA h $g^{-1}$, and the capacity retention rates are 69% and 54%, respectively. In comparison, although the initial specific capacity of the NNCM sample doped with lithium at the alkali metal site is slightly reduced, the capacity retention rate is significantly improved. This is because $Li^+$ and $Na^+$ have the same valence state and will preferentially replace $Na^+$ in the material during the doping process. $Li^+$ has strong polarity and the strong interaction with the substrate makes it difficult for Li at this site to participate in charging. During the discharge process, the theoretical capacity is lost.[33] However, Li doping at the alkali metal sites reduces the ordering of $Na^+$/vacancy to a certain extent and increases the mobility of $Na^+$; in addition, a small part of Li enters the transition metal layer to occupy Mn sites, reducing the concentration of $Mn^{3+}$ and enhancing $TMO_2$. The interaction force between the interlayer elements improves the stability of the structure so that the capacity retention rate of the sample is significantly enhanced. The results show that the addition of Li is positively correlated with the improvement of the capacity retention rate of the cathode material. Fig. 4e shows the midpoint voltage of discharge (MPV) for the pristine and Li-doped electrodes. It can be clearly seen that after 300 cycles, the discharge midpoint voltage decay of NNCM is 2.381 V, while that of [NL]NCM is 2.497 V. Obviously, the alkali-metal-site Li doping improves the cycling stability and mitigates the voltage decay.[34] The [NL]NCM electrode material can still provide an initial specific capacity of 111.7 mA h $g^{-1}$ at 5C, and the capacity retention rate is 69.3% after 500 cycles (Fig. 4f). Fig. 4g compares the cycling performance of NNCM and [NL]NCM electrode materials at 0.2C. The initial discharge-specific capacities of NNCM and [NL]NCM are 156 mA h $g^{-1}$ and 146 mA h $g^{-1}$, and the capacity retention rates after 300 cycles are 45.1% and 66.1%, respectively. Compared with the pristine NNCM, the presence of Li leads to

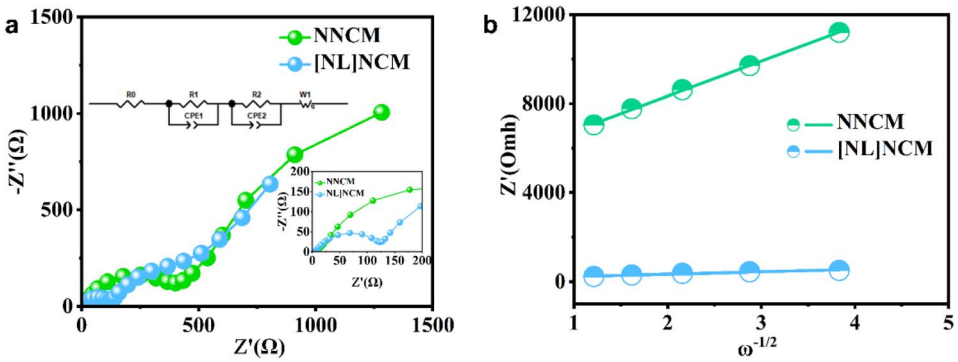


Fig. 5 Kinetics analyses of sodium storage for the [NL]NCM electrode. (a) EIS curves of NNCM and [NL]NCM electrodes. (b) Relationship between real impedance with the low frequencies of the pristine (NNCM) and Li-doped ([NL]NCM) electrodes.

Table 1 Impedance parameters and sodium-ion diffusion coefficient of various electrodes

| Samples | $R_s$ (Ω) | $R_{ct}$ (Ω) | $D_{Na^+}$ ($cm^2\ s^{-1}$) |
|---|---|---|---|
| NNCM | 5.158 | 3511 | $5.822 \times 10^{-15}$ $cm^2\ s^{-1}$ |
| [NL]NCM | 5.173 | 124.3 | $1.838 \times 10^{-12}$ $cm^2\ s^{-1}$ |

a higher capacity retention rate, although the initial capacity of the materials doped with Li at alkali metal sites is slightly lower.

Fig. 5a and b show the electrochemical impedance spectroscopy (EIS) results of the two samples at an open-circuit voltage (OCV), proving that the alkali-metal-site Li-doped material has better rate capability. According to the combined analysis of EIS and Z view software, the two plots consist of two semicircles in the high-frequency range and a straight line in the low-frequency range consisting of the Warburg impedance of Na diffusion in the electrode material.[35] The first semicircle reflects the desolation behavior of sodium ions at the interface, and the second semicircle can be regarded as the charge transfer resistance. The first semicircle of the [NL]NCM is smaller, which indicates that the Na mobility in the electrode material is higher for the Li-doped sample than for the pristine sample. The total impedance of the two parts decreases from 1006 Ω (NNCM) to 633 Ω ([NL]NCM). In summary, alkali metal site Li doping can increase the electronic conductivity and accelerate the migration of sodium ions, thus enhancing the rate capability of the cathode material. The Na-ion diffusion coefficient of the electrode can be calculated using eqn (1) and (2).

$$Z_{re} = R_{ct} + R_s + \sigma_\omega^{-1/2} \quad (1)$$

$$D_{(Na^+)} = \frac{R^2T^2}{2A^2n^2F^4C^2\sigma^2} \quad (2)$$

The $Na^+$ diffusion coefficients for NNCM and [NL]NCM electrodes were calculated as $5.822 \times 10^{-15}$ $cm^2\ s^{-1}$ and $1.838 \times 10^{-12}$ $cm^2\ s^{-1}$, respectively, as shown in Table 1.

These results indicate that Lithium doping facilitates the transport of sodium ions and is an effective method to improve the rate capability of the electrode.

## Conclusions

In summary, we successfully synthesized a novel alkali metal-site Li-doped cathode material and explored the effect of Li substitution on the electrochemical performance of the P2-NNCM composite. The initial discharge-specific capacity of the [NL]NCM electrode at 0.2C (1.5–4.2 V) was 146 mA h $g^{-1}$, and the capacity retention was 66.1% after 300 cycles. With the charging and discharging cycles of the battery, the electrochemical reaction between the electrode material and sodium led to the structural change of the electrode material, and the generation of the solid electrolyte led to the covering of the electrode surface, which reduced the capacity of the battery. Therefore, we designed a P2-type layered cathode material by optimizing the structural modulation and partially replacing the alkali metal site Na with Li. The experimental results showed that Li first enters the alkali metal layer by partially replacing the Na site, and Li, which was not involved in the charging and discharging process, inhibited the ordering of $Na^+$/vacancy, thus enlarging the gap and greatly improving the diffusion rate of $Na^+$. A small portion of Li entered the transition metal layer to replace the Mn site, and highly inhibited the Jahn–Teller activity of $Mn^{3+}$ in synergy with the diatoms (Ni and Co), thus improving the structural stability of the electrode material at high multiplicity, thereby improving the capacity retention rate.

## Data availability

The data that support the findings of this study are available from the corresponding author upon reasonable request.

## Conflicts of interest

The authors declare no competing interests.

## Acknowledgements

This research was supported by the Horizontal Scientific Research Projects (No. 23SL-015) by Shanghai University of Engineering and Technology, and College Research Projects (No. DHXK23002) by Shanghai Donghai Vocational and Technical College.

## References

1 M. Baumann, M. Häringer, M. Schmidt, L. Schneider, J. F. Peters, W. Bauer, *et al.*, Prospective sustainability screening of sodium-ion battery cathode materials, *Adv. Energy Mater.*, 2022, **12**, 2202636.

2 X. Wang, S. Roy, Q. Shi, Y. Li, Y. Zhao and J. Zhang, Progress in and application prospects of advanced and cost-effective iron (Fe)-based cathode materials for sodium-ion batteries, *J. Mater. Chem. A*, 2021, **9**, 1938–1969.

3 C. I. Azambou, O. O. Obiukwu, P. K. Tsobnang, I. T. Kenfack, E. E. Kalu and E. E. Oguzie, Electrochemical performance and structural evolution of layered oxide cathodes materials for sodium-ion batteries: a review, *J. Energy Storage*, 2024, **94**, 112506.

4 J. Wang, Y. F. Zhu, Y. Su, J. X. Guo, S. Chen, H. K. Liu, *et al.*, Routes to high-performance layered oxide cathodes for sodium-ion batteries, *Chem. Soc. Rev.*, 2024, **53**, 4230–4301.

5 Z. Hao, X. Shi, Z. Yang, X. Zhou, L. Li, C. Q. Ma, *et al.*, The distance between phosphate-based polyanionic compounds and their practical application for sodium-ion batteries, *Adv. Mater.*, 2024, **36**, 2305135.

6 J. Xiao, F. Zhang, K. Tang, X. Li, D. Wang, Y. Wang, *et al.*, Rational design of a P2-type spherical layered oxide cathode for high-performance sodium-ion batteries, *ACS Cent. Sci.*, 2019, **5**, 1937–1945.

7 H. Gao, J. Zeng, Z. Sun, X. Jiang and X. Wang, Advances in layered transition metal oxide cathodes for sodium-ion batteries, *Mater. Today Energy*, 2024, **42**, 101551.

8 V. Shipitsyn, R. Jayakumar, W. Zuo, B. Sun and L. Ma, Understanding High-Voltage Behavior of Sodium-Ion Battery Cathode Materials Using Synchrotron X-Ray and Neutron Techniques: A Review, *Batteries*, 2023, **9**, 461–481.

9 X. Wang, X. Yin, X. Feng, Y. Li, X. Dong, Q. Shi, *et al.*, Rational design of $Na_{0.67}Ni_{0.2}Co_{0.2}Mn_{0.6}O_2$ microsphere cathode material for stable and low temperature sodium ion storage, *Chem. Eng. J.*, 2022, **428**, 130990.

10 Y. Zhao, L. Li, Y. Wu, Y. Fang and H. Xie, Progress of the Elements Doped $NaFeO_2$ Cathode Materials for High Performance Sodium-ion Batteries, *ChemistrySelect*, 2021, **6**, 9701–9708.

11 B. Peng, Z. Sun, L. Zhao, J. Li and G. Zhang, Dual-manipulation on P2-$Na_{0.67}Ni_{0.33}Mn_{0.67}O_2$ layered cathode toward sodium-ion full cell with record operating voltage beyond 3.5 V, *Energy Storage Mater.*, 2021, **35**, 620–629.

12 E. Oz, S. Altin and S. Avci, Tunnel/Layer Composite $Na_{0.44}MnO_2$ Cathode Material with Enhanced Structural Stability via Cobalt Doping for Sodium-Ion Batteries, *ACS Omega*, 2023, **8**, 27170–27178.

13 M. Yan, K. Xu and Y. X. Chang, Cu/Ti co-doping boosting P2-type Fe/Mn-based layered oxide cathodes for high-performance sodium storage, *J. Colloid Interface Sci.*, 2023, **651**, 696–704.

14 P. F. Wang, H. R. Yao, X. Y. Liu, J. N. Zhang, L. Gu, X. Q. Yu, *et al.*, Ti-substituted $NaNi_{0.5}Mn_{0.5-x}Ti_xO_2$ cathodes with reversible O3− P3 phase transition for high-performance sodium-ion batteries, *Adv. Mater.*, 2017, **29**, 1700210.

15 C. Tang, W. Lu, Y. Zhang, W. Zhang, C. Cui, P. Liu, *et al.*, Toward Ultrahigh Rate and Cycling Performance of Cathode Materials of Sodium Ion Battery by Introducing a Bicontinuous Porous Structure, *Adv. Mater.*, 2024, **36**, e2402005.

16 Q. Deng, Q. Cheng, X. Liu, C. Chen, Q. Huang, J. Li, *et al.*, 3D porous fluorine-doped $NaTi_2(PO_4)_3$@C as high-performance sodium-ion battery anode with broad temperature adaptability, *Chem. Eng. J.*, 2022, **430**, 132710.

17 P. Lei, S. Li, D. Luo, Y. Huang, G. Tian and X. Xiang, Fabricating a carbon-encapsulated $NaTi_2(PO_4)_3$ framework as a robust anode material for aqueous sodium-ion batteries, *J. Electroanal. Chem.*, 2019, **847**, 113180.

18 J. Huang, L. Xu, D. Ye, W. Wu, S. Qiu, Z. Tang, *et al.*, Suppressing the P2–O2 phase transition of P2-type Ni/Mn-based layered oxide by synergistic effect of Zn/Ti co-doing for advanced sodium-ion batteries, *J. Alloys Compd.*, 2024, **976**, 173397.

19 M. Chen, J. Xiao, W. Hua, Z. Hu, W. Wang, Q. Gu, *et al.*, A Cation and anion dual doping strategy for the elevation of titanium redox potential for high-power sodium-ion batteries, *Angew. Chem.*, 2020, **132**, 12174–12181.

20 Y. Zhao, X. Gao, H. Gao, H. Jin and J. B. Goodenough, Three electron reversible redox reaction in sodium vanadium chromium phosphate as a high-energy-density cathode for sodium-ion batteries, *Adv. Funct. Mater.*, 2020, **30**, 1908680.

21 H. Li, M. Xu, C. Gao, W. Zhang, Z. Zhang, Y. Lai, *et al.*, Highly efficient, fast and reversible multi-electron reaction of $Na_3MnTi(PO_4)_3$ cathode for sodium-ion batteries, *Energy Storage Mater.*, 2020, **26**, 325–333.

22 Y. Xie, E. Gabriel, L. Fan, I. Hwang, X. Li, H. Zhu, *et al.*, Role of lithium doping in P2-$Na_{0.67}Ni_{0.33}Mn_{0.67}O_2$ for sodium-ion batteries, *Chem. Mater.*, 2021, **33**, 4445–4455.

23 L. Yang, X. Li, J. Liu, S. Xiong, X. Ma, P. Liu, *et al.*, Lithium-doping stabilized high-performance P2–$Na_{0.66}Li_{0.18}Fe_{0.12}Mn_{0.7}O_2$ cathode for sodium ion batteries, *J. Am. Chem. Soc.*, 2019, **141**, 6680–6689.

24 F. Li, Y. Tian, Y. Sun, P. Hou, X. Wei and X. Xu, Suppressing the P2−O2 phase transformation and $Na^+$/vacancy ordering of high-voltage manganese-based P2-type cathode by cationic co-doping, *J. Colloid Interface Sci.*, 2022, **611**, 752–759.

25 Y. You, S. Xin, H. Y. Asl, W. Li, P. F. Wang, Y. G. Guo, *et al.*, Insights into the improved high-voltage performance of Li-incorporated layered oxide cathodes for sodium-ion batteries, *Chem*, 2018, **4**, 2124–2139.

26 Y. Zhu, W. Nie, P. Chen, Y. Zhou and Y. Xu, Li-doping stabilized P2-$Li_{0.2}Na_{1.0}Mn_{0.8}O_2$ sodium ion cathode with oxygen redox activity, *Int. J. Energy Res.*, 2020, **44**, 3253–3259.

27 Y. Li, Y. Zhao, X. Feng, X. Wang, Q. Shi, J. Wang, *et al.*, A durable P2-type layered oxide cathode with superior low-temperature performance for sodium-ion batteries, *Sci. China Mater.*, 2022, **65**, 328–336.

28 Y. Xiao, Y. F. Zhu, H. R. Yao, P. F. Wang, X. D. Zhang, H. Li, *et al.*, A stable layered oxide cathode material for high-performance sodium-ion battery, *Adv. Energy Mater.*, 2019, **9**, 1803978.

29 Y. Wang, R. Xiao, Y. S. Hu, M. Avdeev and L. Chen, P2-$Na_{0.6}[Cr_{0.6}Ti_{0.4}]O_2$ cation-disordered electrode for high-rate symmetric rechargeable sodium-ion batteries, *Nat. Commun.*, 2015, **6**, 6954.

30 C. Zhao, Z. Yao, Q. Wang, H. Li, J. Wang, M. Liu, *et al.*, Revealing high Na-content P2-type layered oxides as advanced sodium-ion cathodes, *J. Am. Chem. Soc.*, 2020, **142**, 5742–5750.

31 Y. Li, Q. Shi, X. Yin, J. Wang, J. Wang, Y. Zhao, *et al.*, Construction nasicon-type $NaTi_2(PO_4)_3$ nanoshell on the surface of P2-type $Na_{0.67}Co_{0.2}Mn_{0.8}O_2$ cathode for superior room/low-temperature sodium storage, *Chem. Eng. J.*, 2020, **402**, 126181.

32 J. Y. Hwang, J. Kim, T. Y. Yu and Y. K. Sun, A new P2-type layered oxide cathode with extremely high energy density for sodium-ion batteries, *Adv. Energy Mater.*, 2019, **9**, 1803346.

33 P. Ma, J. Shu, X. Zhao, Y. Cao, L. Wang, G. Chen, *et al.*, The $CrBr_3$ monolayer: two dimension sodium ion battery anode material to characterize state-of-charge by magnetism, *Appl. Surf. Sci.*, 2023, **623**, 157074.

34 R. Yue, F. Xia, R. Qi, D. Tie, S. Shi, Z. Li, *et al.*, Trace Nb-doped $Na_{0.7}Ni_{0.3}Co_{0.1}Mn_{0.6}O_2$ with suppressed voltage decay and enhanced low temperature performance, *Chin. Chem. Lett.*, 2021, **32**, 849–853.

35 A. Laforgue, X. Z. Yuan, A. Platt, S. Brueckner, F. Perrin-Sarazin, M. Toupin, *et al.*, Effects of fast charging at low temperature on a high energy Li-ion battery, *J. Electrochem. Soc.*, 2020, **167**, 140521.